Spatio-temporal dynamics of evapotranspiration on the Tibetan Plateau from 2000 to 2010

2017 Environ. Res. Lett. 12 014011

(http://iopscience.iop.org/1748-9326/12/1/014011)

Environmental Research Letters

LETTERS

Spatio-temporal dynamics of evapotranspiration on the Tibetan Plateau from 2000 to 2010

Lulu Song[1,2], Qianlai Zhuang[2], Yunhe Yin[3], Xudong Zhu[4] and Shaohong Wu[3,5]

[1] Institute of Urban Environment, Chinese Academy of Sciences, Xiamen, 361021, Fujian, People's Republic of China
[2] Department of Earth, Atmospheric and Planetary Sciences, Department of Agronomy, Purdue University, West Lafayette, IN, 47907, United States
[3] Key Laboratory of Land Surface Pattern and Simulation, Institute of Geographic Sciences and Natural Resources Research, Chinese Academy of Sciences, Beijing, 100101, People's Republic of China
[4] Key Laboratory of the Coastal and Wetland Ecosystems, Ministry of Education, Xiamen University, Xiamen 361102, Fujian, People's Republic of China
[5] Author to whom any correspondence should be addressed.

E-mail: wush@igsnrr.ac.cn

Keywords: evapotranspiration, penman–Monteith, net precipitation, tibetan plateau

OPEN ACCESS

RECEIVED
30 September 2016

ACCEPTED FOR PUBLICATION
8 December 2016

PUBLISHED
11 January 2017

Abstract

Evapotranspiration (ET) is a key process of the climate system because it links water, energy and carbon cycles. In this study we modified a Penman–Monteith based algorithm to estimate ET on the Tibetan Plateau at a 1-km spatial resolution for the period 2000–2010 using meteorological and satellite remote sensing data. The results showed that the average annual ET on the Tibetan Plateau was 350.3 mm year^{-1} and decreased from the southeast toward the northwest. The highest ET value was found in open water bodies (680.9 mm year^{-1}) and the lowest ET value was found in open shrubland (254.0 mm year^{-1}). Overall, the inter-annual ET decreased from 2000 to 2010 and there was significant negative ET trend over 42% of the region, primarily in the northwest of the Tibetan Plateau. Relative humidity was the dominant factor in controlling long-term variations of ET in the arid northwest plateau. But under moist conditions, leaf area index or temperature drove ET. In addition, *P*-ET on the Tibetan Plateau significantly increased and about 37% of the region showed strong positive *P*-ET trend primarily in the central of the Tibetan Plateau. The positive *P*-ET trend in four seasons suggested that the Tibetan Plateau might have become wetter during the past decade.

1. Introduction

Evapotranspiration (ET), which is the sum of water lost from various land surfaces through evaporation, from the stomata of plants through transpiration, and from snow cover through sublimation, plays a key role in land surface energy balance and hydrological cycle (Oki and Kanae 2006, Trenberth *et al* 2009, Vinukollu *et al* 2011). The hydrological cycle is expected to accelerate with global warming and there has been an increasing trend in ET as revealed by a review of historical trends in hydrologic variables (Huntington 2006). However, our understanding of the relative magnitudes and spatial patterns of ET changing trends is limited due to sparse ET observation networks. An accurate assessment of temporal and spatial dynamics of ET in response to climate change is essential for projecting potential changes in the global hydrological cycle.

The water transfer processes involved in ET depend on atmospheric demand and moisture supply (Jung *et al* 2010, Seneviratne *et al* 2010). And there are numerous factors driving ET, including radiation, vapour-pressure deficit, temperature, soil moisture and stomatal conductance (influenced by leaf area and vegetation coverage) (Hu *et al* 2013, Wang *et al* 2010, Jung *et al* 2010, Chen *et al* 2014, Seneviratne *et al* 2010), making accurate assessment of ET a challenge. ET is routinely measured at flux towers, but the high spatial heterogeneity of ET limits the application of flux tower measurements to regional or global assessments (Anderson *et al* 2003, Wang *et al* 2010).

Several satellite-based approaches are available to quantify ET at large scales, including (1) empirical

methods (Jung *et al* 2010, Jin *et al* 2011, Zhang *et al* 2007, Yin *et al* 2013); (2) surface energy balance methods, such as Surface Energy Balance System (SEBS; Su 2002); (3) physical models, such as Penman-Monteith algorithm (Monteith 1965, Penman 1948). The empirical methods, based on statistical relationships between measured ET and eco-environmental parameters, are convenient for ET estimation on global or regional scales. However, uncertainties in the empirical coefficients for different ecosystems or regions pose a challenge for the accurate assessment of ET (Jin *et al* 2011). The surface energy balance models are theoretically sound, but their performances are constrained by the estimation of sensible heat flux and soil heat flux (Cleugh *et al* 2007). Among these modeling methods, the Penman-Monteith algorithm and its varieties have been widely used to estimate ET at regional or global scales (Cleugh *et al* 2007, Mu *et al* 2007, 2011, Zhang *et al* 2009, 2010, Yuan *et al* 2010), due to its more mechanistic representation of ET processes by introducing aerodynamic and surface resistances. Mu *et al* (2011) took a further step to improve the Penman-Monteith algorithm by developing more realistic formulations of stomatal conductance, aerodynamic resistance and boundary layer resistance. This modification of the Penman–Monteith algorithm had been proved to be biophysically sound and rigorous for estimating ET at regional scales (Jung *et al* 2010, Vinukollu *et al* 2011, Li *et al* 2014, Chen *et al* 2014).

The Tibetan Plateau (TP) is very sensitive to climate change (Zheng 1996, Immerzeel *et al* 2010). As indicated by previous studies (Liu and Chen 2000, Wang *et al* 2008, Wu *et al* 2007), the warming trend over the plateau might have led to glacier retreat (Yao *et al* 2004) and permafrost degradation (Wu and Zhang 2010, Yang *et al* 2010). These warming-induced changes will greatly affect the ET processes over the plateau. Until now, most of the ET studies on the TP focused on ET at river basin (Zhang *et al* 2007, Xue *et al* 2013) or site scales (Hu *et al* 2009, 2013, Zhu *et al* 2013, Yao *et al*, 2008, Gu *et al* 2005). Only a few studies conducted large-scale ET assessments on the TP. For example, Yin *et al* (2013) investigated ET dynamics with Lund-Potsdam-Jena dynamic vegetation model and concluded that the increasing ET trend over the last 30 years was linked with increased precipitation. To get a more accurate ET assessment on the TP, a continuous ET record with a high spatio-temporal resolution is needed. Furthermore, the assessment of ET dynamics on the TP is also limited by the lack of our knowledge on the ET controls and net precipitation (precipitation minus ET) at regional scales.

The objectives of this study are: (1) to evaluate the performance of the modified Penman–Monteith based algorithm; (2) to quantify the spatial and temporal patterns of ET among different land-cover types on the TP from 2000 to 2010; (3) to investigate the dominant environment variables; and (4) to explore the response patterns of both ET and net precipitation to climate change during the period.

2. Methods and data sources

2.1. Study site

The Tibetan Plateau (TP) (75°E–105°E, 25°N–40°N), the highest (average elevation >4000 m) and largest (>2.5 million km^2) highland in the world, is located in western China and covers most of the Tibet Autonomous Region and Qinghai province, as well as small portions of western Sichuan province, southwestern Gansu province, northern Yunnan province and Xinjiang Autonomous Region (figure 1). Most areas of the TP are characterized with an arid/semiarid climate. The mean annual precipitation is 473 mm, ranging from 1000 to 50 mm. The mean annual temperature is 3.8 °C, ranging from −15 °C to 10 °C. The patterns of precipitation and temperature result in an increase in aridity from southeast to northwest of the TP. More than 60% of the plateau is alpine grasslands, which includes alpine meadows, alpine steppes and alpine desert. The TP is rich in lakes, glaciers, and wetlands, and is the main source of several major rivers in Asia.

2.2. Models

2.2.1. The modified Penman–Monteith algorithm.

Our ET algorithm is a revision of the algorithm proposed by Mu *et al* (2011) which is based on the well-known Penman–Monteith equation (Penman 1948, Monteith 1965) (hereafter called PM-Mu (2011))

$$\lambda \mathrm{ET} = \Delta(R_{\mathrm{net}} - G_{\mathrm{flux}}) + \frac{\rho C_p \mathrm{VPD}/r_{\mathrm{a}}}{\Delta + \gamma(1 + r_{\mathrm{s}}/r_{\mathrm{a}})} \quad (1)$$

where λET (W m^{-2}) is the latent heat flux (LE), λ (J kg^{-1}) is the latent heat of vaporization, R_{net} (W m^{-2}) is the net incoming radiation to the land surface, G_{flux} (W m^{-2}) is the soil heat flux, ρ (kg m^{-3}) is the air density, C_p (J kg^{-1} K^{-1}) is the specific heat capacity of air, VPD (Pa) is the vapour-pressure deficit, Δ (Pa K^{-1}) is the slope of the saturate vapor pressure curve, γ is the psychrometric constant, r_{a} (s m^{-1}) is the aerodynamic resistance and r_{s} (s m^{-1}) is the surface (or canopy) resistance.

Similar with PM-Mu (2011), we estimated evaporation from soil ($\lambda E_{\mathrm{SOIL}}$), wet plant ($\lambda E_{\mathrm{wet\_c}}$) and transpiration from plant ($\lambda E_{\mathrm{trans}}$) separately. And details of estimation are as follows.

The R_{net} was calculated as equation (2).

$$R_{\mathrm{net}} = (1 - \alpha) \times R_{\mathrm{sw}} + (1 - 0.26\exp^{(-7.77 \times 10^{-4} \times T^2)} - 0.97) \times \sigma \times (273.15 + T)^4 \quad (2)$$

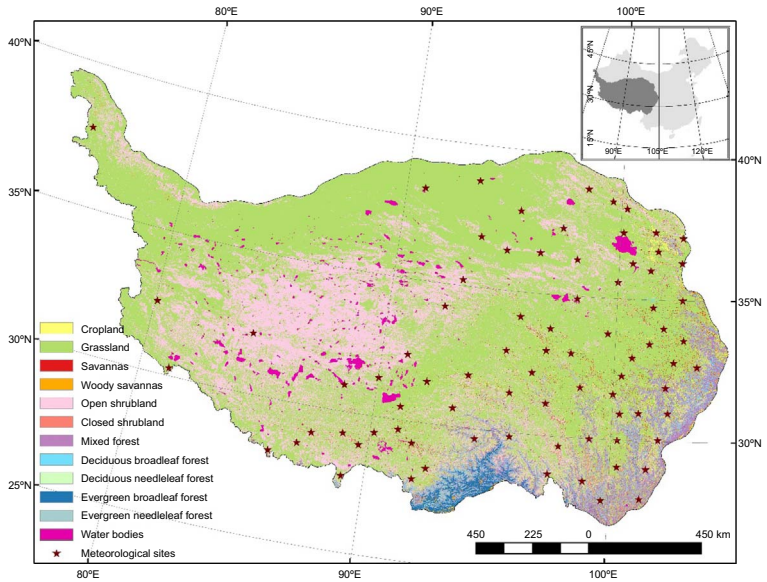

Figure 1. Map of land-cover types derived from the MODIS (UMD classification scheme) and meteorological sites on the Tibetan Plateau.

where α is MODIS albedo, R_{sw} (W m^{-2}) is the incoming shortwave radiation and σ (5.67 × 10^{-8} W m^{-2} k^{-4}) is Stefan–Boltzmann constant.

Different from PM-Mu (2011), we modified the G_{flux} with following equations recommended by Frempong (1983):

For water surfaces,

$$G_{flux} = 0.26 \times R_{net} \tag{3}$$

For other land-cover types,

$$G_{flux} = R_{net} \times \left[\Gamma_{canopy} + (1 - f_c)(\Gamma_{soil} - \Gamma_{canopy})\right] \tag{4}$$

where Γ is the ratio of soil heat flux to the net radiation. The values of Γ for soil and canopy are 0.315 (Kustas and Daughtry 1990) and 0.05 (Monteith 1973), respectively.

The fractional vegetation cover information (f_c), estimated from MODIS FPAR (the Fraction of Absorbed Photosynthetically Active Radiation), was used to partition the available energy ($R_{net} - G_{flux}$) between soil and vegetation.

$$\begin{aligned} \mathrm{As} &= (1 - f_c)(R_{net} - G_{flux}) \\ \mathrm{Ac} &= f_c(R_{net} - G_{flux}) \\ f_c &= \mathrm{FPAR} \end{aligned} \tag{5}$$

As in PM-Mu (2011), we separated dry canopy surface from the wet by F_{wet} to calculate evaporation from the wet canopy surface and moist bare soil surface.

$$F_{wet} = \begin{cases} 0.0 & \mathrm{RH} < 70\% \\ \mathrm{RH}^4 & 70\% \le \mathrm{RH} \le 100\% \end{cases} \tag{6}$$

The evaporation from wet canopy surface was calculated as equation (7).

$$\lambda E_{wet\_c} = \frac{(\Delta \times \mathrm{Ac} + \rho \times C_p \times \mathrm{VPD}/r_{a\_c}) \times F_{wet}}{\Delta + \gamma \times (1 + r_{s\_c}/r_{a\_c})} \tag{7}$$

$$\begin{aligned} r_{s\_c} &= \frac{\rho \times C_p}{\mathrm{gl\_e\_wv} \times \mathrm{LAI} \times F_{wet}} \\ \mathrm{rhc} &= \frac{1.0}{\mathrm{gl\_sh} \times \mathrm{LAI} \times F_{wet}} \\ \mathrm{rrc} &= \frac{\rho \times C_p}{4.0 \times \sigma \times T_{air}^3} \\ r_{a\_c} &= \frac{\mathrm{rhc} \times \mathrm{rrc}}{\mathrm{rhc} + \mathrm{rrc}} \end{aligned} \tag{8}$$

where rhc (s m^{-1}) is the wet canopy resistance to sensible heat, rrc (s m^{-1}) is the resistance to radiative heat transfer through air, gl_sh (s m^{-1}) is leaf conductance to sensible hear per unit leaf area index (LAI), gl_e_wv (m s^{-1}) is leaf conductance to evaporated water vapor per unit LAI, and T_{air} is the air temperature.

The plant transpiration was calculated as equation (9).

$$\lambda E_{trans} = \frac{(\Delta \times \mathrm{Ac} + \rho \times C_p \times \mathrm{VPD}/r_a) \times (1 - F_{wet})}{\Delta + \gamma \times (1 + r_s/r_a)} \tag{9}$$

$$\begin{aligned} r_a &= \frac{\mathrm{rh} \times \mathrm{rr}}{\mathrm{rh} + \mathrm{rr}} \\ \mathrm{rh} &= \frac{1.0}{\mathrm{gl\_sh}} \end{aligned} \tag{10}$$

The value of rr was equal to the rrc in equation (8).

$$
\begin{aligned}
r_s &= 1/c_c \\
\mathrm{Gs1} &= C_L \times m(T_{min}) \times m(\mathrm{VPD}) \times r_{\mathrm{corr}} \\
\mathrm{Gcu} &= r_{\mathrm{corr}} \times 0.1 \times 10^{-4} \\
\mathrm{Gs2} &= \mathrm{gl\_sh} \\
C_c &= \begin{cases} \dfrac{\mathrm{Gs2} \times (\mathrm{Gs1} + \mathrm{Gcu})}{\mathrm{Gs1} + \mathrm{Gs2} + \mathrm{Gcu}} \times \mathrm{LAI} \times (1.0 - F_{\mathrm{wet}}) & (\mathrm{LAI} > 0.0, (1.0 - F_{\mathrm{wet}}) > 0.0) \\ 0.0 & (\mathrm{LAI} = 0.0, (1.0 - F_{\mathrm{wet}}) = 0.0) \end{cases} \\
r_{\mathrm{corr}} &= \frac{1.0}{\dfrac{101300}{P_a} \times \left(\dfrac{T + 273.15}{293.15}\right)^{1.75}}
\end{aligned}
\tag{11}
$$

where C_c is the canopy conductance, which is derived from stomatal conductance (Gs1), leaf cuticular conductance (Gcu) and leaf boundary-layer conductance (Gs2), P_a is the atmospheric pressure, $m(T_{\mathrm{min}})$ and $m(\mathrm{VPD})$ are multipliers that limits potential stomatal conductance, which were calculated using the same equations in Mu *et al* (2011). Based on the characteristics of TP, we calibrated $\mathrm{VPD}_{\mathrm{close}}$, the biome-specific critical value of VPD at which canopy stomata are completely closed, and C_L, the mean potential stomatal conductance per unit leaf area, to be 3600 Pa and 0.0065 m s^{-1} for grasslands based on the *in-situ* measurements of ET. The other biome property parameters were taken from Mu *et al* (2011).

Soil evaporation ($\lambda E_{\mathrm{SOIL}}$) was calculated in equation (12).

$$
\begin{aligned}
\lambda E_{\mathrm{wet\_soil}} &= \frac{\left(\Delta \times \mathrm{As} + \rho \times C_p \times \mathrm{VPD}/r_{\mathrm{as}}\right) \times F_{\mathrm{wet}}}{\Delta + \gamma \times r_{\mathrm{tot}}/r_{\mathrm{as}}} \\
\lambda E_{\mathrm{soil\_POT}} &= \frac{\left(\Delta \times \mathrm{As} + \rho \times C_p \times \mathrm{VPD}/r_{\mathrm{as}}\right) \times (1 - F_{\mathrm{wet}})}{\Delta + \gamma \times r_{\mathrm{tot}}/r_{\mathrm{as}}} \\
\lambda E_{\mathrm{soil}} &= \lambda E_{\mathrm{wet\_soil}} + \lambda E_{\mathrm{soil\_POT}} \times \left(\frac{\mathrm{RH}}{100}\right)^{\mathrm{VPD}/\beta}
\end{aligned}
\tag{12}
$$

where β was set as 200 in PM-Mu (2011), and was revised as 50 in the improved algorithm. Details in calculating r_{as}, r_{tot} and other parameters are the same with Mu *et al* (2011).

2.2.2. Evaporation from snow.

Since snow pack is important for water resources and hydrology, we considered the evaporation over snow based on the characteristics of TP. And Penman equation was used:

$$
\lambda E_{\mathrm{snow}} = \frac{\Delta \times (R_{\mathrm{net}} - G) + \rho \times C_p \times (e_{\mathrm{sat}} - e)/r_a}{\Delta + \gamma}
\tag{13}
$$

where r_a is the aerodynamic resistance and expressed as a power function of wind speed at height 2 m (U_2):

$$
r_a = \frac{208}{U_2}
\tag{14}
$$

The transpiration over snow covered plants was assumed to be negligible since stomata closes at freezing temperature (Vinukollu *et al* 2011).

2.2.3. Evaporation from water bodies.

Besides the snow evaporation, we also considered the evaporation over water bodies. And the Priestley–Taylor equation (Priestley and Taylor 1972) was used:

$$
\lambda E_{\mathrm{water}} = \alpha \frac{\Delta (R_{\mathrm{net}} - G)}{\Delta + \gamma}
\tag{15}
$$

where α is calculated by the equation recommended by Er-Raki *et al* (2010):

$$
\alpha = -0.014\mathrm{RH} + 2.24
\tag{16}
$$

Finally, the total daily ET was the sum of different parts:

For water surfaces,

$$
\lambda E = \lambda E_{\mathrm{water}} + \lambda E_{\mathrm{snow}}
\tag{17}
$$

For other land-cover types,

$$
\lambda E = \lambda E_{\mathrm{wet\_c}} + \lambda E_{\mathrm{trans}} + \lambda E_{\mathrm{soil}} + \lambda E_{\mathrm{snow}}
\tag{18}
$$

The model time step was set to 8 days because the satellite products were calculated as 8-day composites.

2.3. *Data*

2.3.1. Meteorological inputs.

Daily *in-situ* meteorological datasets from 2000 to 2010, including air temperature (T_{air}), relative humidity (RH), wind speed (U) and precipitation (P) from 109 meteorological stations (figure 1), were downloaded from China Meteorological Administration website (http://cdc.cma.gov.cn/index.jsp).

2.3.2. Satellite inputs.

Remote sensing datasets used in this study included: 1) 1-km 8-day Collection 4 MODIS land cover type 2 (MOD12Q1); 2) 1-km 8-day MODIS Collection 5 FPAR/LAI (MOD15A2); 3) 1-km 16-day MODIS Collection 5 albedo (MCD43B3); 4) 500-m 8-day MODIS Collection 5 snow cover fraction (MOD10A2); 5) 1-km 8-day MODIS global ET data calculated by PM-Mu (2011) (MOD16A2); 6) 1° × 1° daily CERES-SSF R_{sw} product. All detailed information of MODIS and CERES products is available at the

website http://modis.gsfc.nasa.gov and http://ceres.larc.nasa.gov/order_data.php.

2.3.3. Eddy covariance data.

To validate the revised model, we used *in-situ* measurements of LE at two eddy covariance sites. One is located at Haibei alpine grassland station in Qinghai (37°36′N101°20′E; 3160 m a.s.l.). The other is located at Damxung grassland station, north of Lhasa city, Tibet (30°51′N, 91°05′E; 4333 m a.s.l.). The study periods extended from January 2003 to December 2004 for Haibei station and from July 2003 to December 2005 for Damxung station. We aggregated the half-hourly flux observations into daily values, and those days with more than 20% missing half-hourly data were excluded.

2.3.4. Pre-processing input data.

The satellite products contain cloud-contaminated or missing data. All missing or unreliable data were processed using method proposed by Zhao *et al* (2005) with a software package MATLAB10.0. The daily values of meteorological measurements and R_{sw} were averaged to 8-day interval and spatially interpolated to 1-km with inverse distance weighting method (Lu and Wong 2008).

The tower measured data are given every 30 min, and for each 30-min time period, ET (mm 30 min^{-1}) was calculated as:

$$\mathrm{ET} = \frac{\mathrm{LE} \times 60 \times 30}{\lambda} \tag{19}$$

$$\lambda = (2.501 - 0.002361 \times T_{\mathrm{air}}) \times 10^6 \tag{20}$$

2.3.5. Model performance and trend analysis.

Root mean square error (RMSE), mean bias error (MBE) as well as observation (R^2) were calculated to analyze the difference between the modeled simulations and observations.

$$\mathrm{RMSE} = \sqrt{\frac{1}{n}\sum_{i=1}^{n}(\mathrm{ET}_{\mathrm{obs}} - \mathrm{ET}_{\mathrm{mod}})^2} \tag{21}$$

$$\mathrm{MBE} = \frac{1}{n}\sum_{i=1}^{n}(\mathrm{ET}_{\mathrm{obs}} - \mathrm{ET}_{\mathrm{mod}}) \tag{22}$$

where $\mathrm{ET}_{\mathrm{obs}}$ and $\mathrm{ET}_{\mathrm{mod}}$ is observed and modeled value, respectively; and n is the total number of observations.

Linear trend analysis was used to quantify the inter-annual, seasonal and each pixel trend of the ET (y_t).

$$y_t = y_0 + bx_t \tag{23}$$

Statistically significant differences were set as $p < 0.1$ unless otherwise stated. Correlation (r) was calculated to determine which environmental factor explained most of the variation of ET.

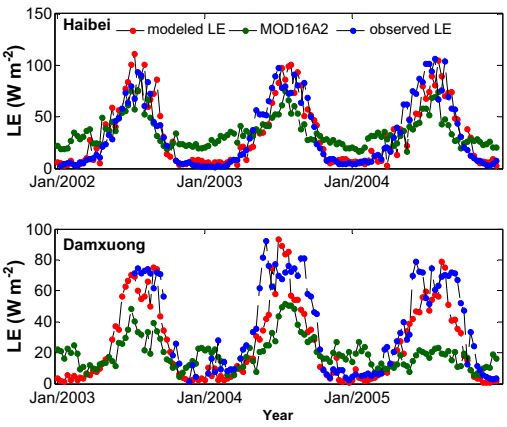

Figure 2. Comparisons of the seasonal dynamics between modeled LE, MOD16A2 and measured LE.

3. Results

3.1. Model performance

The ET averaged over the 5 × 5 1-km^2 pixels surrounding each site is compared with the tower ET observations. Two tower sites with available LE are used to compare ET seasonal variability between our modeled LE flux and MOD16A2. Compared with MOD16A2, the ET estimates from our revised model are much lower in winter, but much closer to the observations in summer. For these two tower sites, the revised model shows generally favorable agreement with the tower observations and captures the seasonality of observed LE (figure 2). Overall, the modified model reduces MBE from 0.03 W m^{-2} using the Mu *et al* (2011) algorithm to 0.007 W m^{-2}, improves LE accuracy (RMSE) from 25.7 W m^{-2} to 15.8 W m^{-2}, and enhances LE correlation (R^2) from 0.36 to 0.76 (figure 3).

3.2. Spatial patterns of ET

The mean annual ET on the TP estimated by the modified PM-Mu (2011) is 350.3 ± 139.9 mm year^{-1} and the spatial ET distribution corresponds to variations in precipitation, available energy and temperature on the plateau. The largest ET exhibits in the southeast whereas small ET exhibits in the dry and lower temperature regions especially in the northwest. Spatially, the distribution ET estimated by modified model matches well with MOD16A2 (figure 4), although spatially-averaged ET of the MOD16A2 is about 111.1 mm higher.

Furthermore, the spatial ET distribution is also associated with distributions of the major land-cover types (figure 5). As expected, the highest average ET value is found in open water bodies which is 680.9 mm year^{-1}; and open shrubland have the lowest ET, which is 254.0 mm year^{-1}. The ET values for other land-cover types lie between the two extremes. ET of croplands is generally higher than that of grasslands, which due to irrigation in croplands.

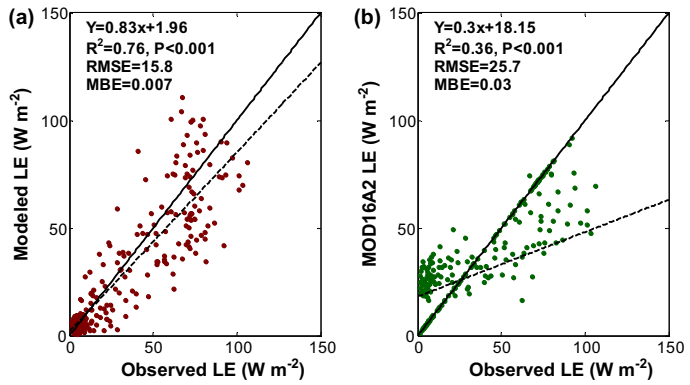

Figure 3. Comparison between measured LE and modeled LE, and MOD16A2.

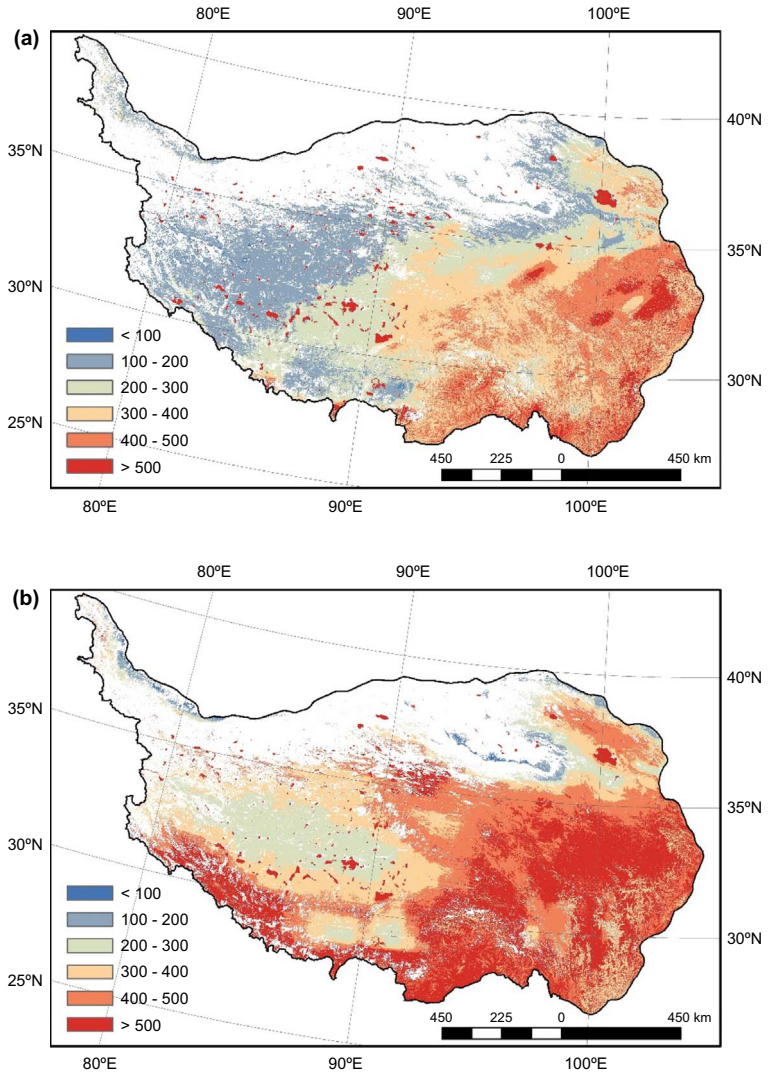

Figure 4. Spatial distribution of mean annual ET estimations (mm year^{-1}) (*a*) and MOD16A2 (mm year^{-1}) (*b*) from 2000 to 2010 on the Tibetan Plateau.

The mean seasonal distribution patterns of ET from 2000 to 2010 show distinct fluctuations (figure 6). Temporally, in spring (March–May), most parts of southeast TP show significantly high ET values because the forest ecosystems, distributing in these regions with mild temperatures and moist conditions during the spring, start to grow. ET goes to the highest level in summer (June–August) because of high precipitation, dense vegetation and intensive radiation. In autumn (September–November), the ET drops as vegetation senesced and radiation declined. The majority of the TP has very low ET in winter (December–February) because of low available energy, temperature, and stomatal conductance.

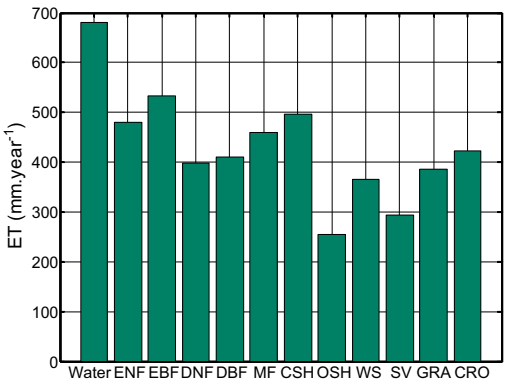

Figure 5. Average total amount ET estimations of different land-cover types from 2000 to 2010 on the Tibetan Plateau. Water: water bodies; ENF: evergreen needleleaf forest; EBF: evergreen broadleaf forest; DNF: deciduous needleleaf forest; DBF: deciduous broadleaf forest; MF: mixed forest; CSH: closed shrubland; OSH: open shrubland; WS: woody savannas; SV: savannas; GRA: grassland; CRO: cropland.

3.3. Inter-annual variability of ET

Spatially, there is considerable variability in ET trends. Approximately 42% of the plateau with strong negative ET inter-annual variability occurs over grasslands, open shrublands and deciduous needleleaf forest, while 0.5% of the region shows obvious positive ET trends over evergreen broadleaf forest (figure 7(*a*)). As a whole, ET significantly decreases on TP for the 2000–2010 period (4.7 mm year^{-1}, $p < 0.001$) (figure 7(*b*)).

We calculated the correlation between environmental factors (R_{sw}, LAI, RH, T_{air}, FPAR, and Albedo) and ET in each pixel. And the results show that mean annual RH ($r = 0.72$), LAI ($r = 0.62$) and T_{air} ($r = 0.58$) are important factors that affect ET variations overall the TP from 2000 to 2010. Generally, for dry conditions (northwestern Tibetan Plateau), ET contributes to RH, but under moist conditions (southeastern Tibetan Plateau), LAI or T_{air} drives ET (figure 8).

3.4. Changes in net precipitation

Theoretically, ET should be less than precipitation over a relative long time period. To validate the ET results and assess the water balance changes, we calculated the net precipitation (*P*-ET). The results show that ET is less than *P* spatially and a mean annual *P*-ET value of 112.2 mm year^{-1} from 2000 to 2010 is estimated on the TP. Spatially, *P*-ET presents a similar distribution pattern with respect to ET. The *P*-ET is generally low in arid regions of the northwest TP, whereas relatively high *P*-ET is located downstream of Brahmaputra (figure 9).

Contrary to ET, the inter-annual *P*-ET increases significantly (5.0 mm year^{-1}, $p < 0.1$) and varies between 68.5 and 150.1 mm year^{-1} from 2000 to 2010 (figure 10(*b*)). Regionally, about 37% areas showing strong positive *P*-ET trends primarily occur in the central of the TP, and only 2% areas present strong negative *P*-ET trends (figure 10(*a*)). Positive *P*-ET trends generally occur over grasslands and open shrublands, while negative trends occur within forests regions of the domain (table 1).

In addition, both regional average ET and *P*-ET show seasonal changes during the 11-year period (figure 11). The ET shows significant ($p < 0.1$) negative variability for all four seasons, with the largest ET decreases in summer followed by spring and autumn. Opposite to ET seasonal pattern, *P*-ET presents significant positive variability ($p < 0.01$) in winter, with slightly increasing *P*-ET in spring, summer and autumn. The positive *P*-ET trends in four seasons indicate that the TP became wetter during the past decade.

4. Discussion

4.1. Model performance and uncertainties

The accurate ET estimation at the diurnal time scale in this study demonstrated satisfactory predictive capabilities of the modified PM-Mu (2011) model. Compared with the MODIS ET product, our modified model illustrated better performance at the tower sites (figures 2 and figure 3). There were two reasons that resulted in the better performance of the modified model. On the one hand, the parameters in this study were locally validated while those of the MODIS ET were only tested by AmeriFlux eddy covariance tower sites. On the other hand, the different input driving variables were used, i.e. meteorological data from CMA was used in this study while re-analyses meteorological data from GMAO was used in MODIS ET. The GMAO climate data tended to have high uncertainties in winter (Zhao *et al* 2005).

Potential sources of uncertainties in ET estimates could come from the algorithm itself. Although many studies had confirmed the good performance of the Penman–Monteith model and contributed to its parameterization (Cleugh *et al* 2007, Mu *et al* 2007, 2011, Zhang *et al* 2009, 2010, Yuan *et al* 2010, Li *et al* 2014, Chen *et al* 2014), not claiming completeness, some improvements can be made to the modified PM-Mu (2011). For example, as the source of water cycle, *P* was not an input parameter to constrain ET. In addition, since soil moisture was the main limiting factor for the plant physiological processes, the effect of soil water condition on canopy stomatal conductance should add to the model (Hu *et al* 2013). Another limitation of the ET algorithm was that the effect of high CO_2 and nitrogen induced stomatal closure on stomatal resistance had not been considered in estimating ET. Furthermore, some key parameters were given with empirical values, which may cause large deviation.

In addition, uncertainties in ET estimates could also come from the input driving data. Due to inaccessibility, the complex terrain, sparse meteorological stations and higher elevation (>4500 m) in the western TP, the ET estimates may be negatively

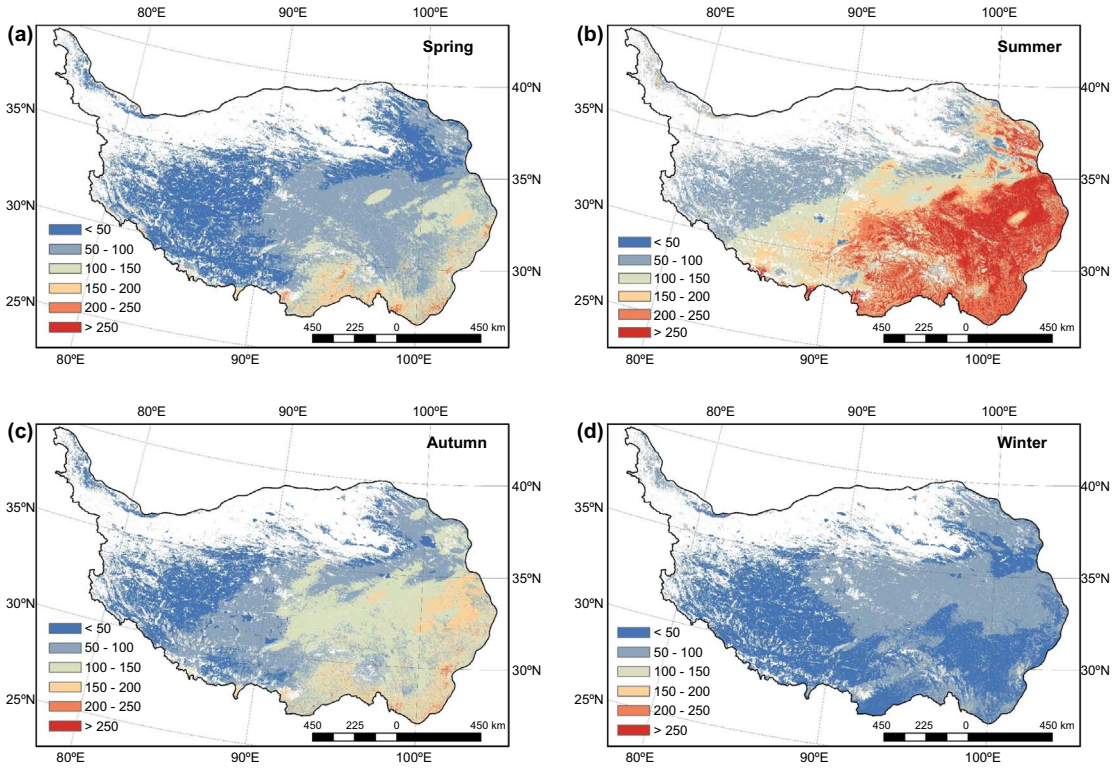

Figure 6. Seasonal distributions of average ET (mm season^{-1}) from 2000 to 2010 on the Tibetan Plateau.

impacted by the inherited interpolation meteorological inputs. In addition, uncertainties from MODIS LAI/FPAR, albedo and land-cover data can introduce biases to ET estimates. For example, MODIS LAI tended to be higher than measurements (Wang *et al* 2004) and the bias of MODIS land-cover data were in range of 20%–30% (Strahler *et al* 2002). Moreover, evaporation from open water bodies were likely underestimated due to the inability of 1-km MODIS land-cover information to resolve rivers on the TP.

Generally, validation of the estimations with eddy flux LE measurements posed challenges. Firstly, uncertainties may be introduced by comparing measured ET with the estimated from the 5 × 5 1-km^2 pixels due to differences in tower footprints (Anderson *et al* 2003). Second, the eddy covariance flux towers had a problem with energy balance closure because of complexity in wind variation, footprint representation, and sampling variability (Twine *et al* 2000). The energy balance was rarely closed resulting in non-closure on the order of 20%–30%. Therefore, the best model would subsequently explain only an R^2 of around 0.70–0.80, which was generally what our model produces.

4.2. Variations of ET on the Tibetan Plateau

The distribution pattern and ranges of variations in ET in this study were consistent with previous studies (Chen *et al* 2014, Yao *et al* 2013, Li *et al* 2014, Yin *et al* 2013). The annual mean ET was highest in the relatively humid regions, intermediate in temperate regions and the lowest in cold and arid regions. The reduction in ET toward the northwest was corresponding to climate resources patterns and distributions of the major biome types on the TP (figure 4).

Although the assessments of ET had been made by numerous models, ET inter-comparison studies showed large uncertainties in global or regional ET estimates (Vinukollu *et al* 2011, Chen *et al* 2014). For example, Chen *et al* (2014) compared eight ET models, including five empirical and three process-based models, and found that the process-based models performed better than the empirical models. Although eight models indicated similar spatial patterns, there were substantial differences in the magnitude and inter-annual variability of ET, which may be because of differences in model-dominated variables. The modified PM-Mu (2011) model in this study demonstrated similar results with other satellite-based physical process models in magnitude and inter-annual variation. For example, Yao *et al* (2013) studied the terrestrial ET in China for ten years (2001–2010) based on a modified Priestley–Taylor model and reported that the estimated ET was 320 mm year^{-1}on the TP. Li *et al* (2014) estimated that the mean annual ET on the TP was 345 mm year^{-1} with RS-Mu model when used 1982–2009 satellite records to calculate ET over China. Jung *et al* (2010) showed that the estimated mean ET value from 1982 to 2008 was about 350 mm year^{-1} on the TP based on the global evaluated ET map. Vinukollu *et al* (2011) used three process based models to estimate ET on the global scale and their results indicated the mean annual ET varied from 150 mm to 600 mm on the TP.

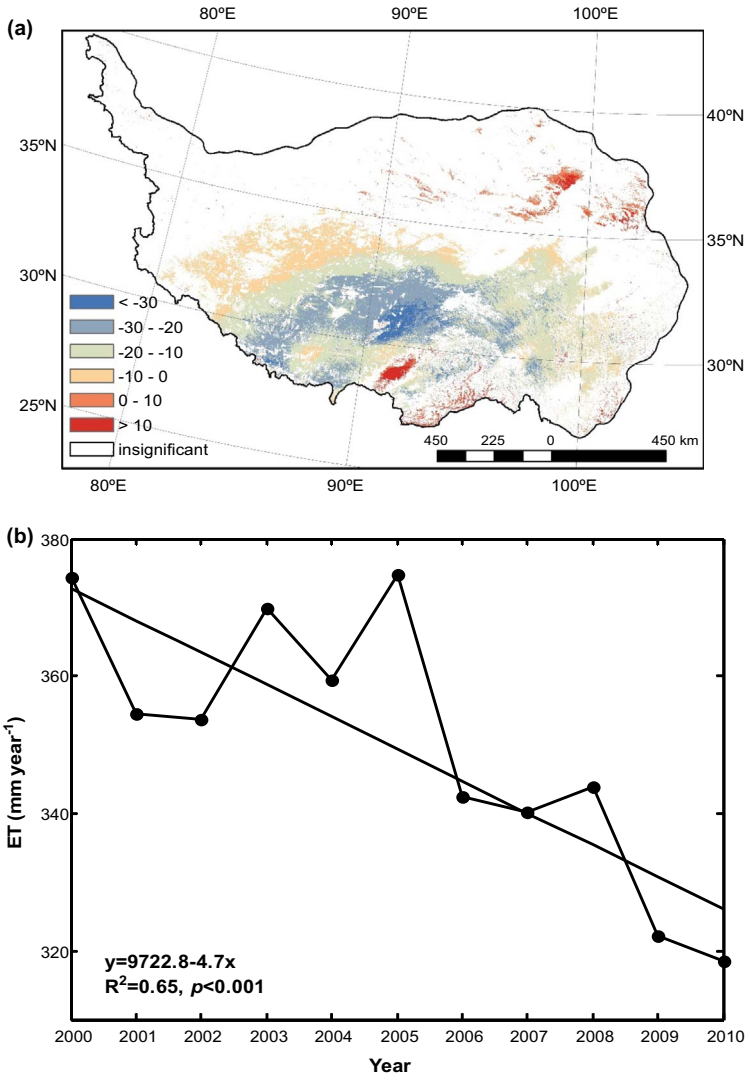

Figure 7. Spatial distribution of inter-annual variability in ET (mm year^{-1}) (a) and annual time series of ET (b) from 2000 to 2010 on the Tibetan Plateau.

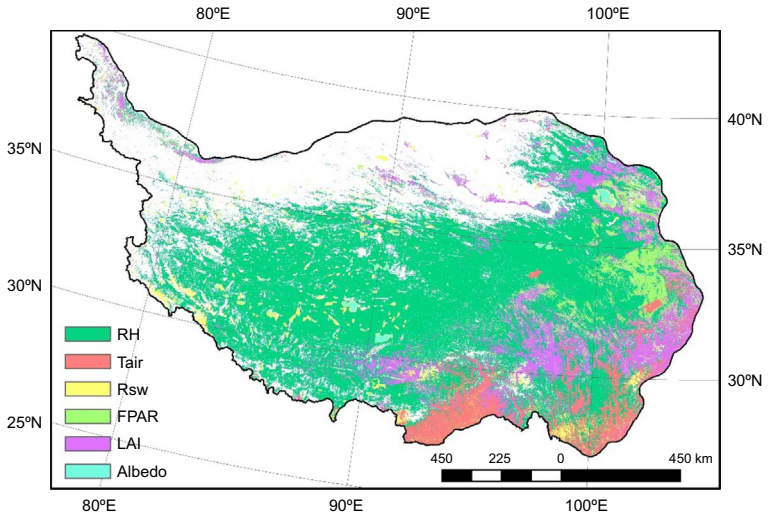

Figure 8. Spatial distribution of most related driving variables for annual ET from 2000 to 2010 on the Tibetan Plateau.

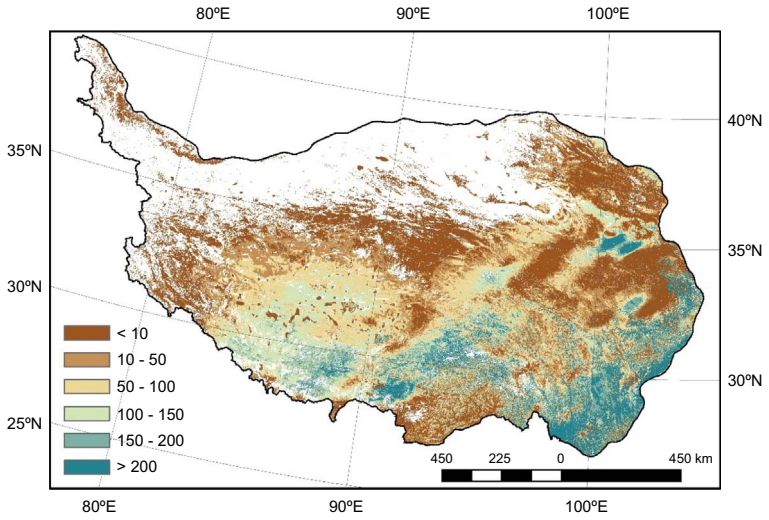

Figure 9. Spatial distribution of mean annual *P*-ET (mm year^{-1}) from 2000 to 2010 on the Tibetan Plateau.

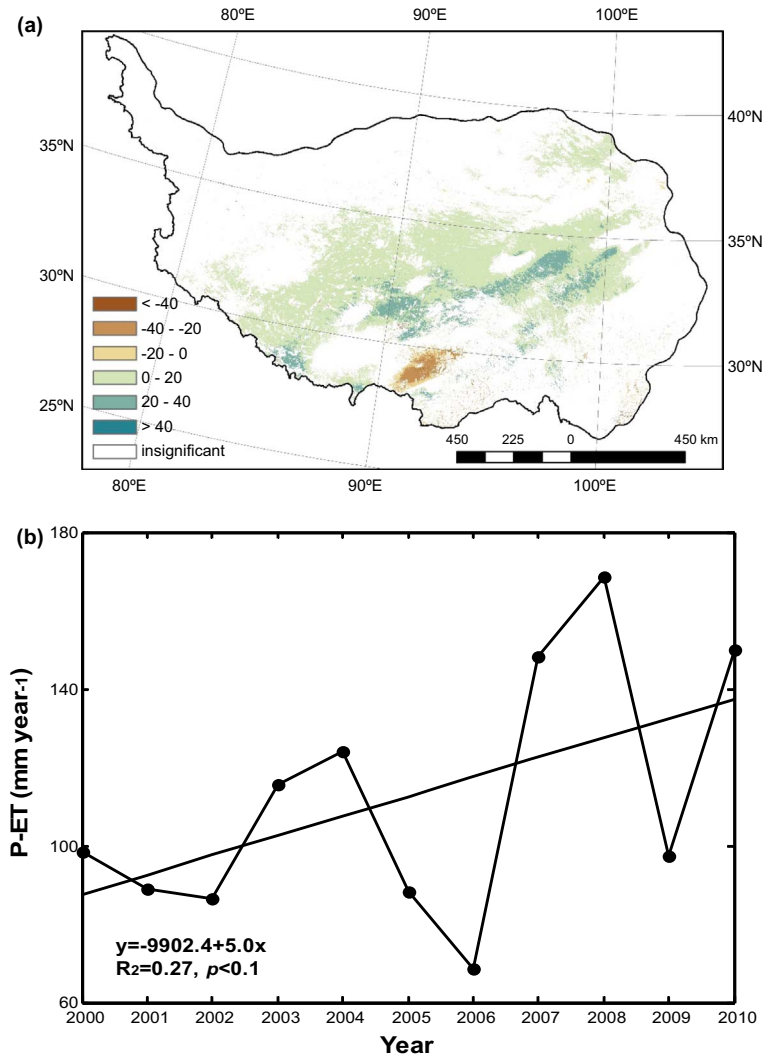

Figure 10. Spatial distribution of inter-annual variability in *P*-ET (mm year^{-1}) (*a*) and annual time series of *P*-ET (*b*) during 2000–2010 on the Tibetan Plateau.

Table 1. Inter-annual variability of ET and *P*-ET from 2000 to 2010 for different land-cover types on the Tibetan Plateau.

Land cover types	Area percentage (%)	Inter-annual ET variability (mm year^{-1})	Inter-annual P-ET variability (mm year^{-1})
Water bodies	1.53	25.22**	−25.20*
Evergreen needleleaf forest	2.84	−0.78	−10.01
Evergreen broadleaf forest	0.86	4.85**	−3.23
Deciduous needleleaf forest	0.04	−3.76**	−0.58
Deciduous broadleaf forest	0.67	−2.17	0.44
Mixed forest	3.38	−0.41	−3.32
Closed shrubland	0.59	−5.42***	0.85
Open shrubland	25.20	−7.28***	6.67**
Woody savannas	0.85	−0.51	−2.27
Savannas	0.64	−1.49	0.99
Grassland	62.59	−8.48***	8.35**
Cropland	0.82	−1.22	−0.41

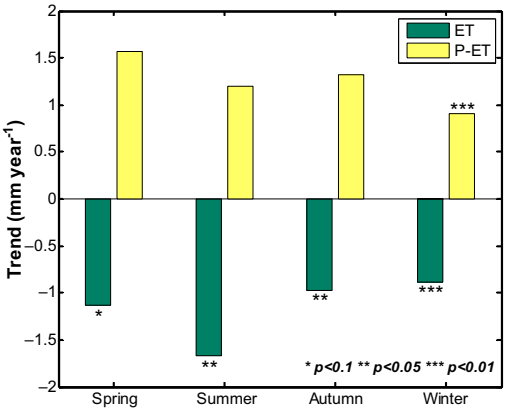

Figure 11. Seasonal variability of regional average ET and *P*-ET from 2000 to 2010 on the Tibetan Plateau.

Generally, the ET variability is either induced by atmospheric energy demand or by terrestrial moisture-supply (Jung *et al* 2010). ET will respond to atmospheric demand (e.g. temperature) in well-watered regions, where warming is expected to promote increase in ET and precipitation leading to a general acceleration of the water cycle (Huntington 2006). However, moisture-supply will turn to be the dominant driving factor if the soils are too dry. Study of Jung *et al* (2010) demonstrated that the warming-induced increasing ET disappeared after the last big El Niño event in 1998. Similar with previous studies (Wang *et al* 2010, Yao *et al* 2013, Li *et al* 2014, Chen *et al* 2014), the declining ET in our study was not consistent with the expected acceleration of the hydrological cycle. Our TP-ET estimates suggested that the inter-annual ET decreased from 2000 to 2010 with a linear trend of 4.7 mm year^{-1}, coinciding with regional permafrost thawing (Wu and Zhang 2010, Yang *et al* 2010) and vegetation degradation (Harris 2010). It was found that the largest regional contributions to the declining trend since 2000 originated from the northwest of the TP in which ET was limited by moisture-supply, indicated here by RH (figure 8). The decreasing RH also contributed to inter-annual and seasonal decreased variations in ET. In these dry regions, lower ET was expected to feed back to the atmosphere and increased atmospheric dryness. However, under relatively moist conditions (southeast of TP), dependencies of ET on LAI and T_{air} appeared to be largely independent of RH (figure 8). Lower LAI and T_{air} indicated less leaves and lower canopy conductance, thus decreased in ET (Wang *et al* 2010, Chen *et al* 2014).

The net precipitation (*P*-ET) describes moisture flux between the land surface and the atmosphere. Changes in *P*-ET could affect local atmospheric moisture content and regional climate. Our results showed that *P*-ET close to zero in northwest, which confirmed the droughts in this region (figure 9). And relatively small difference between *P* and ET implies a strong sensitivity of water supplies to relatively small changes in *P* or ET. In addition, our findings of increasing water supply since 2000 coincide with increase in runoff and lake level on the TP (Zhang *et al* 2011).

5. Conclusions

ET remains one of the greatest unknowns within the global energy, water and carbon cycles. To better understand the spatio-temporal dynamics of ET on the Tibetan Plateau, we have modified the PM-Mu (2011) model to estimate the Tibetan Plateau's ET on an 8-day time scale. Overall, the mean annual ET was 350.3 mm year^{-1} and decreased from southeast to northwest of Tibetan Plateau. The inter-annual ET showed a decreasing variability from 2000 to 2010. High negative ET rates were found in the northwest of the Tibetan Plateau. RH was the dominant factor in controlling long-term variations of ET in arid northwest plateau. However, in the moist southeast plateau, variations of ET were primarily controlled by T_{air} and LAI. Contrary to the ET variability, *P*-ET presented significant positive trends all season and an increasing pattern from 2000 to 2010. This indicates that the Tibetan Plateau became wetter during the past decade.

Acknowledgments

The authors thank Dr Peili Shi from Institute of Geographical Science and Natural Resources Research, Chinese Academy of Sciences, for providing latent heat flux data for the Damxung site of the ChinaFlux network. This research is partly supported through projects to QZ by the NASA Land Use and Land Cover Change program (NASA-NNX09AI26G), Department of Energy (DE-FG02-08ER64599), National Science Foundation (NSF-1028291 and NSF- 0919331), and the NSF Division of Information & Intelligent Systems (IIS-1028291). This research is

also supported by the Key Program of the National Natural Science Foundation of China (41530749) and the National Natural Science Foundation of China (41571043). The computing is supported by Rosen Center of high performance computing at Purdue.

References

Anderson M C, Kustas W P and Norman J M 2003 Upscaling and downscaling—a regional view of the soil-plant-atmosphere continuum *Agron. J.* **95** 1408–23

Chen Y *et al* 2014 Comparison of satellite-based evapotranspiration models over terrestrial ecosystems in China *Remote Sens.Environ.* **140** 279–93

Cleugh H A, Leuning R, Mu Q Z and Running S W 2007 Regional evaporation estimates from flux tower and MODIS satellite data *Remote Sens. Environ.* **106** 285–304

Emanuel R E, D'Odorico P and Epstein H E 2007 Evidence of optimal water use by vegetation across a range of North American ecosystems *Geophys. Res. Lett.* **34** L07401

Er-Raki S *et al* 2010 Assessment of reference evapotranspiration methods in semi-arid regions: can weather forest data be used as alternate of ground meteorological parameters *J. Arid Environ.* **74** 1587–96

Fisher J B, Tu K P and Baldocchi D D 2008 Global estimates of the land-atmosphere water flux based on monthly AVHRR and ISLSCP-IIdata, validated at 16 FLUXNET sites *Remote Sens. Environ.* **112** 901–19

Frempong E 1983 Diel aspects of the thermal structure and energy budget of a small English lake *Freshwater Biol.* **13** 89–102

Gu S, Tang Y, Cui X, Kato T, Du M, Li Y and Zhao X 2005 Energy exchange between the atmosphere and a meadow ecosystem on the Qinghai-Tibetan Plateau *Agric. Forest Meteorol.* **129** 175–85

Harris R B 2010 Rangeland degradation on the Qinghai-Tibetan Plateau: a review of the evidence of its magnitude and causes *J. Arid Environ.* **74** 1–12

Hu Z *et al* 2009 Partitioning of evapotranspiration and its controls in four grassland ecosystems: application of a two-source model *Agric. Forest Meteorol.* **149** 1410–20

Hu Z, Li S, Yu G, Sun X, Zhang L, Han S and L Y 2013 Modeling evapotranspiration by combing a two-source model, a leaf stomatal model, and a light-use efficiency model *J. Hydrol.* **50** 186–92

Huntington T G 2006 Evidence for intensification of the global water cycle: review and synthesis *J. Hydrol.* **319** 83–95

Immerzeel W W, Van Beek L P H and Bierkens M F P 2010 Climate change will affect the Asian water towers *Science* **328** 1382–5

Jin Y F, Randerson J T and Goulder M L 2011 Continental-scale net radiation and evapotranspiration estimated using MODIS satellite observation *Remote Sens. Environ.* **115** 2302–19

Jung M *et al* 2010 Recent decline in the global land evapotranspiration trend due to limited moisture supply *Nature* **467** 951–4

Kustas W P and Daughtry C S T 1990 Estimation of the soil heat-flux net-radiation ratio from spectral data *Agric. Forest Meteorol.* **49** 205–23

Li X *et al* 2014 Estimation of evapotranspiration over the terrestrial ecosystems in China *Ecohydrology* **7** 139–49

Liu X and Chen B 2000 Climatic warming in the Tibetan plateau during recent decades *Int. J. Climatol.* **20** 1729–42

Lu G Y and Wong D W 2008 An adaptive inverse-distance weighting spatial interpolation technique. *Comput. Geosci.* **34** 1044–55

Monteith J L 1965 Evaporation and environment *Symp. Soc. Exp. Biol.* **19** 205–34

Monteith J L 1973 *Principles of Environmental Physics* (London: Edward Arnold)

Mu Q, Heinsch F A, Zhao M and Running S W 2007 Development of a global evapotranspiration algorithm based on MODIS and global meteorology data *Remote Sens. Environ.* **111** 519–36

Mu Q, Zhao M and Running S W 2011 Improvements to a MODIS global terrestrial evapotranspiration algorithm *Remote Sens. Environ.* **115** 1781–800

Oki T and Kanae S 2006 Global hydrological cycles and world water resources. *Science* **313** 1068–72

Penman H L 1948 Natural Evaporation from open water, bare soil and grass *Proc. R. Soc. London* **193** 120–45

Priestley C H B and Taylor R J 1972 On the assessment of surface heat flux and evaporation using large-scale parameters *Mon. Weather Rev.* **100** 81–92

Seneviratne S I, Corti T, Davin E L, Hirschi M, Jaeger E B, Lehner I, Orlowsky B and Teuling A J 2010 Investigating soil moisture-climate interactions in a changing climate: a review *Earth-Sci. Rev.* **99** 125–61

Strahler A H, Friedl M, Zhang X, Hodges J, Cooper C S A and Baccini A 2002 The MODIS land cover and land cover dynamics products *Presentation at Remote sensing of the Earth's Environment from Terra in L'Aquila Italy*

Su Z 2002 The surface energy balance system (SEBS) for estimation of turbulent fluxes *Hydrol. Earth Syst. Sc.* **6** 85–99

Sun G *et al* 2011 Upscaling key ecosystem functions across the conterminous United States by a water-centric ecosystem model *J. Geophys. Res.: Atmos.* **116** G00J05

Trenberth K E, Fasullo J T and Kiehl J 2009 Earth's global energy budget *Bull. Amer. Meteor. Soc.* **90** 311–23

Twine T E *et al* 2000 Correcting eddy-covariance flux underestimates over a grassland *Agric. Forest Meteorol.* **103** 279–300

Vinukollu R K, Wood E F, Ferguson C R and Fisher J B 2011 Global estimates of evapotranspiration for climate studies using multi-sensor remote sensing data: Evaluation of three process-based approaches *Remote Sens. Environ.* **115** 801–23

Wang B, Bao Q, Hoskins B, Wu G and Liu Y 2008 Tibetan Plateau warming and precipitation changes in East Asia *Geophys. Res. Lett.* **35** L14702

Wang K C, Dickinson R E, Wild M and Liang S L 2010 Evidence for decadal variation in global terrestrial evapotranspiration between 1982 and 2002: 2 *Results J. Geophys. Res.* **115** D2027

Wang Y *et al* 2004 Evaluation of the MODIS LAI algorithm at a coniferous forest site in Finland *Remote Sens. Environ.* **91** 114–27

Wu Q and Zhang T 2010 Changes in active layer thickness over the Qinghai-Tibetan Plateau from 1995 to 2007 *J. Geophys. Res.* **115** D09107`

Wu S, Yin Y, Zheng D and Yang Q 2007 Climatic trends over the Tibetan Plateau during 1971-2000 *J. Geophys. Res.* **17** 141–51

Xue B, Wang L, Li X, Yang K, Chen D and Sun L 2013 Evaluation of evapotranspiration estimates for two river basins on the Tibetan Plateau by a water balance method *J. Hydrol.* **492** 290–7

Yang M, Nelson F E, Shiklomanov N I, Guo D and Wan G 2010 Permafrost degradation and its environmental effects on the Tibetan Plateau: a review of recent research *Earth-Sci. Rev.* **103** 31–44

Yao T, Wang Y, Liu S, Pu J, Shen Y and Lu A 2004 Recent glacial retreat in High Asia in China and its impact on water resource in Northwest China *Sci China Ser. D-Earth Sci.* **47** 1065–75

Yao Y J *et al* 2013 MODIS-driven estimation of terrestrial latent flux in China based on a modified Priestley-Taylor algorithm *Agric. Forest Meteorol.* **171–172** 187–202

Yao J, Zhao L, Ding Y, Gu L, Jiao K, Qiao Y and Wang Y 2008 The surface energy budget and evapotranspiration in the Tanggula region on the Tibetan Plateau *Cold Reg. Sci. Technol.* **52** 326–40

Yin Y, Wu S, Zhao M, Zheng D and Pan T 2013. Modeled effects of climate change on actual evapotranspiration in different eco-geographical regions in the Tibetan Plateau *J. Geogr. Sci.* **23** 195–207

Yuan W P *et al* 2010 Global estimates of evapotranspiration and gross primary production based on MODIS and global meteorology data *Remote Sens. Environ.* **114** 1416–31

Zhang G, Xie H, Kang S, Yi D and Ackley S F 2011 Monitoring lake level changes on the Tibetan Plateau using ICES at altimetry data 2003-2009 *Remote Sens. Environ.* **115** 1733–42

Zhang K, Kimball J S, Mu Q Z, Jones L A, Goetz S J and Running S W 2009 Satellite based analysis of northern ET trends and associated changes in the regional water balance from 1983 to 2005 *J. Hydrol.* **379** 92–110

Zhang K, Kimball J S, Nemani R R and Running S W 2010 A continuous satellite-derived global record of land surface evapotranspiration from 1983 to 2006 *Water Resour. Res.* **46** W09522

Zhang Y, Liu C, Tang Y and Yang Y 2007 Trends in pan evaporation and reference and actual evapotranspiration across the Tibetan Plateau *J. Geophys. Res.* **112** D12110

Zhao M, Heinsch F A, Nemani R and Running S W 2005 Improvements of the MODIS terrestrial gross and net primary production global data set *Remote Sens. Environ.* **95** 164–76

Zheng D 1996 The system of physic-geographical regions of the Qinghai-Xizang (Tibet) Plateau *Sci. China Ser. D-Earth Sci.* **39** 410–7

Zhu G, Su Y, Li X, Zhang K and Li C 2013 Estimating actual evapotranspiration from an alpine grassland on Qinghai-Tibetan Plateau using a two-source model and parameter uncertainty analysis by Bayesian approach *J. Hydrol.* **476** 42–51